

# Flaticulation: Laser Cutting Joints with Articulated Angles

Chiao Fang\*  
National Taiwan University  
Taipei, Taiwan  
chiao.fang@hci.csie.ntu.edu.tw

Vivian Hsinyueh Chan\*  
National Taiwan University  
Taipei, Taiwan  
vivian.chan@hci.csie.ntu.edu.tw

Lung-Pan Cheng  
National Taiwan University  
Taipei, Taiwan  
lung-pan.cheng@hci.csie.ntu.edu.tw



**Figure 1:** *Flaticulation* is a method to laser cut joints that clutch two cut-in-place pieces at designated articulated angles. The key is the special T-patterns on the shared edge of the two pieces. This method allows unfolded 3D polygonal models to be cut and assembled easily as the joints hold pieces together and provide users haptic cues at the right angle. We use *Flaticulation* to produce not only static objects such as polyhedrons with different numbers of faces and a low-poly bunny but also objects with detent mechanisms such as a reconfigurable headpiece and a mouse with detent buttons.

## ABSTRACT

We present *Flaticulation*, a method to laser cut joints that clutch two cut-in-place flat boards at designated articulated angles. We discover special T-patterns added on the shared edge of two pieces allowing them to be clutched at a bending angle. We analyze the structure and propose a parametric model regarding the T-pattern under laser cutting to predict the joint articulated angle. We validate our proposed model by measuring real prototypes and conducting stress-strain analysis to understand their structural strength.

\*Both authors contributed equally to this research.

Permission to make digital or hard copies of all or part of this work for personal or classroom use is granted without fee provided that copies are not made or distributed for profit or commercial advantage and that copies bear this notice and the full citation on the first page. Copyrights for components of this work owned by others than ACM must be honored. Abstracting with credit is permitted. To copy otherwise, or republish, to post on servers or to redistribute to lists, requires prior specific permission and/or a fee. Request permissions from [permissions@acm.org](mailto:permissions@acm.org).  
UIST '22, October 29–November 2, 2022, Bend, OR, USA  
© 2022 Association for Computing Machinery.  
ACM ISBN 978-1-4503-9320-1/22/10...\$15.00  
<https://doi.org/10.1145/3526113.3545695>

Finally, we provide a user interface for our example applications, including fast assembling unfolded 3D polygonal models and adding detent mechanisms for functional objects such as a mouse and reconfigurable objects such as a headpiece.

## CCS CONCEPTS

• **Hardware** → **Emerging technologies**; • **Human-centered computing** → *Interactive systems and tools*.

## KEYWORDS

Personal fabrication, laser-cut joints, articulated angles, assembly

## ACM Reference Format:

Chiao Fang, Vivian Hsinyueh Chan, and Lung-Pan Cheng. 2022. *Flaticulation: Laser Cutting Joints with Articulated Angles*. In *The 35th Annual ACM Symposium on User Interface Software and Technology (UIST '22)*, October 29–November 2, 2022, Bend, OR, USA. ACM, New York, NY, USA, 16 pages. <https://doi.org/10.1145/3526113.3545695>

## 1 INTRODUCTION

Laser cutting is one of the most popular fabrication methods for personal fabrication and rapid prototyping. It fabricates faster than 3D printing while being more precise and with less yield loss than milling. Users iterate their designs on 2D drawings and send them to a laser cutter to cut readily prepared materials (medium-density fiberboard (MDF), acrylic, ABS, etc.) into real pieces. Since laser cutters only cut in 2D, forming complex 3D models requires extra effort in designing mounting joints and hands-on assembling.

To facilitate fabrication of 3D objects using laser cutters, previous works have provided interfaces to embed joints into designs [41] or direct conversion from 3D models into various laser-cuttable plans such as cubes [3, 4], mesh joinery [8, 21, 32], lamination [19, 36], and kirigami/origami patterns [6] for easy hands-on assembling. Various laser-cutting patterns have been introduced to ensure that cut pieces can be properly assembled using the same laser-cut files on different laser cutters regardless of their variant in the laser cutting kerf, i.e., the burned-away material [26, 29]. Researchers also have looked into nesting laser-cut pieces to facilitate fast hands-on assembly [2], or using defocused laser to fold or weld materials automatically without hands-on assembling [22, 36].

Among these techniques, joints such as finger joints, T-joints, cross joints, and mesh joinery has been commonly incorporated in many laser-cut designs [5, 29, 41]. However, these joints require two pieces to be connected perpendicularly to be clutched tightly. Otherwise, users have to use clamps or adhesives to temporarily hold pieces at an angle before assembling their supporting parts. In the meantime, these joints cannot be cut in place, i.e., the two connecting pieces have to be laid out separately to prevent the laser cutting kerf from losing the fit.

In this paper, we discover new joint patterns that enable two cut-in-place pieces to be clutched together by just folding them to an articulated angle, providing an easier way to assemble unfolded 3D polygonal models and detent mechanisms to be added into laser-cut objects.

### 1.1 Flaticulation

*Flaticulation* is a method to laser cut joints that clutch two cut-in-place flat boards at designated articulated angles. The key to the method is 2 types of special T-patterns as shown in Figure 2: (a)  $<\theta$ -T-pattern, which limits the boards from being folded more than an angle  $\theta$ . (b)  $>\theta$ -T-pattern, which on the contrary, prevents the boards from being folded back flat at an angle  $\theta$ .

An *articulated joint* is formed by putting these 2 types of T-patterns on a shared edge, as shown in Figure 3. With the constraints from these 2 types, the two cut-in-place pieces can be clutched at the articulated angle  $\theta$  when simply folding them inward along the edge. In addition, combining the  $>\theta$ -T-pattern with the lattice hinge results in a *detent hinge*, which has a detent right at the articulated angle  $\theta$ .

Flaticulation uses both articulated joints and detent hinges to ease the assembling process of unfolded 3D polygonal models and provide a new laser-cut detent mechanism. We provide a user interface for Flaticulation and introduce it by walking through the process of making a polygonal mouse that has click buttons out of a laser cutter in the following section.

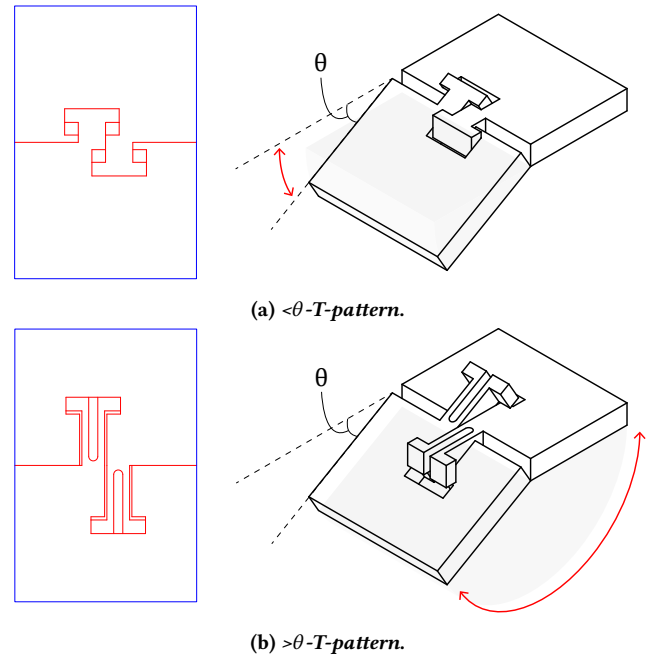


Figure 2: The 2 special T-patterns of Flaticulation.

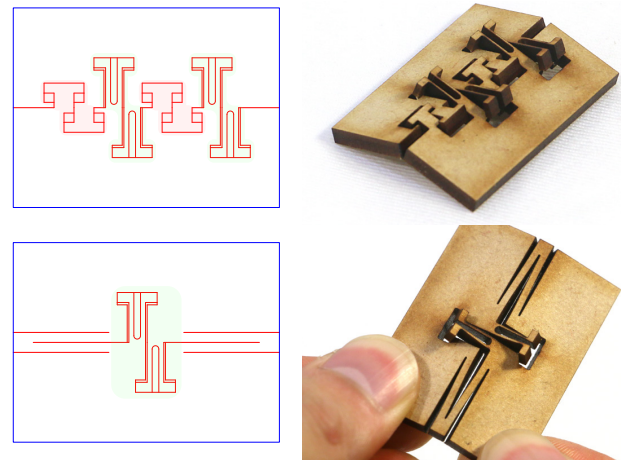
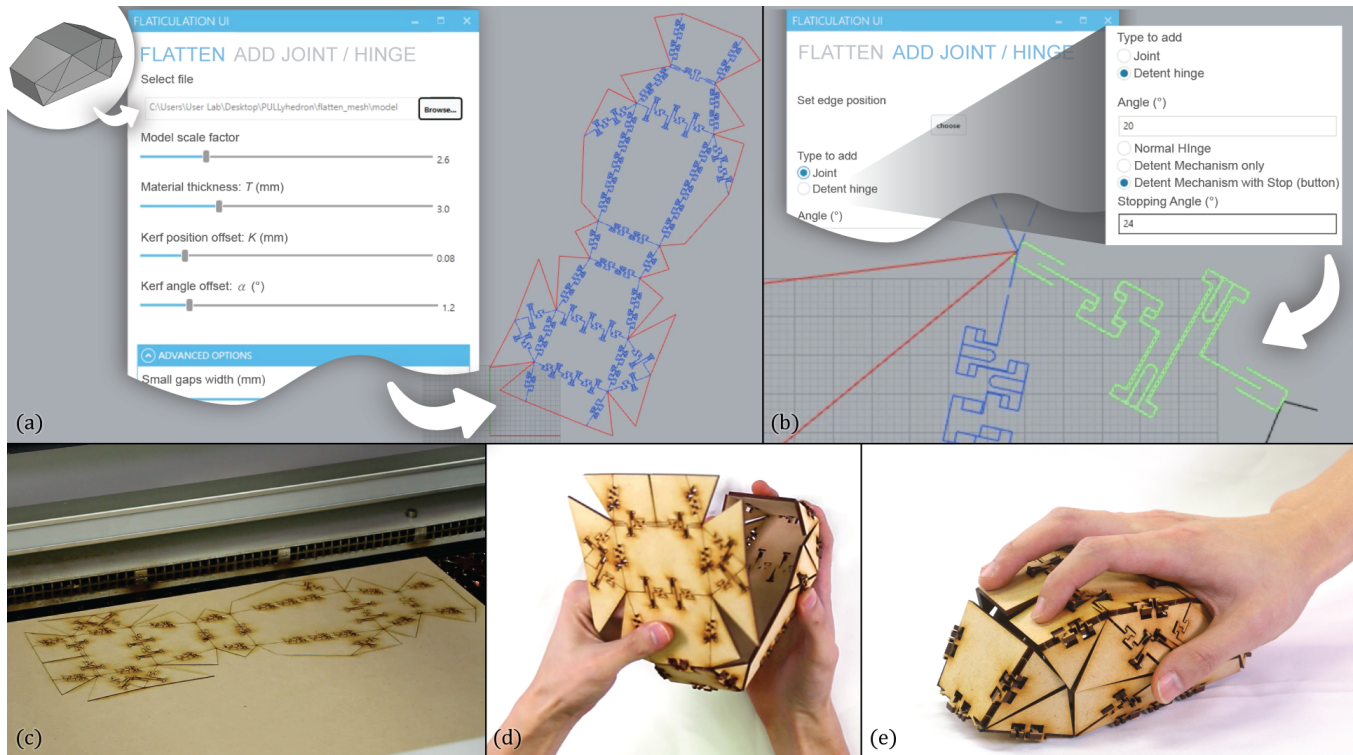


Figure 3: Combining both  $<\theta$  and  $>\theta$  T-patterns results in an articulated joint. Combining  $>\theta$ -T-patterns with the lattice hinge results in a detent hinge.

### 1.2 Using Flaticulation

Figure 4 shows the complete flow of making a mouse out of a laser cutter using Flaticulation. The user starts by making a low-poly mouse model in 3D modeling software. The user then loads the model into our Flaticulation Rhino plugin (Figure 4a). Our plugin automatically unfolds the model into a 2D laser-cuttable plane while recording all articulated angles between all polygons before unfolding. According to the recorded articulated angles, customized laser cutter setting, and flattening settings, our plugin adds corresponding articulated joints into the 2D plan. The user



**Figure 4:** (a) Our Flaticulation Rhino plugin automatically unfolds a user-loaded 3D model and adds corresponding articulated joints on a 2D plan. (b) The user can manually select to use articulated joints or detent hinges and adjust the T-pattern parameters on new or existing edges. (c) The user laser cuts the final 2D plan and (d) assembles the model by folding and clutching all pieces at the right angles. (e) The user clicks the button on the mouse to test the laser-cut detent.

examines the 2D plan and finds the button parts to add detent hinges. After selecting one of the button edges, the user manually changes the articulated joint to the detent hinge. The user further adjusts the T-pattern parameters to tune the detent strength, starting and stopping angles (Figure 4b). Finally, the user cuts the 2D plan on an MDF using a laser cutter (Figure 4c) and finishes assembling the clickable mouse by simply folding pieces to clutch at the right angles (Figure 4d and e).

### 1.3 Contribution

The core contribution of this work is the 2 types of T-patterns that allow 2 cut-in-place pieces to be clutched at an articulated angle. Using these patterns, we derive laser-cuttable articulated joints and detent hinges and wrap them as Flaticulation, a method for fabricating pieces with articulated angles using laser cutting. We further provide a user interface for Flaticulation that allows users to produce easy-to-assemble laser-cut plans for 3D polygonal objects with detent mechanisms. To support our core contribution, we conducted geometry analysis and sorted out a parametric model regarding the laser cutting kerf for the laser-cut T-patterns to clutch at the correct articulated angle. In addition, we evaluated the angular error and the strength of articulated joints produced by Flaticulation under different angles, stress directions, materials,

and thickness. Finally, we built example objects using Flaticulation to showcase its use cases and gain insights into its potential issues. Our contribution as a whole spans from the fundamental understanding of our original method to its pragmatic use.

## 2 RELATED WORK

Carpentry joinery, a part that joins two or more separated wood-work pieces, has a long history in wooden constructions [14] as well as art and crafts [33]. It is an ancient divide-and-conquer technique that allows people to build large and complex objects that are difficult to produce in one piece by assembling small and simple pieces. Terrie Noll reviews joint techniques and provides a detailed guide to carpentry joinery [23]. More knowledge of carpentry joinery has been compiled in recent years through more building guides [10, 25]. Along with modern electrical tools such as Dremel, less effort is required for people to make carpentry joinery to build objects without glue or screws.

Researchers have also worked on the topological optimization of joints in interlocking assemblies. DESIA [37], for example, is a framework for designing interlocking assemblies that allow graph analysis to be performed to optimize parts arrangement. MOCCA [38] is another framework that optimizes cone joints for assemblies with a variety of geometric forms. Researchers also have proposed a way to decompose 3D models into small joining polygons while

maintaining the model’s recognizable shape to ease the assembling process [7]. These works bring in computational models into carpentry joinery, making the computer a new tool that enables people to design more efficient, more configurable, or more durable interlocking objects with less trials and error.

With rocket-rising computation power and commercialization of computer numeric control (CNC) machines such as 3D printers and laser cutters, recent research has looked into providing user interfaces that integrate with computational models for interactive design. More factors in the interaction process such as fabrication constraints from fabrication machines have been brought into consideration, which has been called fabrication-aware design. We selectively introduce works that are related to joint design as follows. Yao et al. [40] propose an interactive joint design tool specifically for 3D printed free-form decorative joints [21]. Digital joinery for hybrid carpentry [20] proposes a user interface for carpenters to create woodwork furniture combining 3D printed joints to support oblique angles that are hard to achieve by traditional carpentry joints. Tsugite [18] is a modeling interface designed for a 3-axis CNC milling machine to create custom joints.

Fabrication-aware design not only appears in 3D printing, but researchers also have looked into laser cutting as well. Due to the 2D nature of most laser cutting technology, it inherently requires joinery to form 3D objects. Joinery [41] summarizes recent laser-cut joints and proposes user interfaces to facilitate the fabrication of 6 types of joints. Finger joint is one joinery that is commonly used in laser-cutting. Since finger joints do not have articulated angles, researchers have proposed using cubes as basic units to form objects [3] More work has been put into overcoming the laser cutting kerf that affects the fit of joinery [26, 29], and taking fast and auto assembling into consideration in the process of converting 3D models to 2D laser-cut plans [2, 27, 28].

Another common joinery is to use planar cross-sections to interlock laser-cut pieces. FlatFitFab [21] is an interactive interface for creating a planar section model to be laser-cut and fabricated. SketchChair [30] generates planar-cross-section chairs from a 2D sketch. crdbrd [13] generates planar section laser-cut files from 3d models. Mesh Joinery [8] proposes a technique to produce angular planar cross-sections for 3D constructions. Schwartzburg et al. take the geometric constraints imposed by fabrication and assembly and the rigidity of the resulting structure into consideration to generate planar-cross-section 2D plans from a 3D model.

Researchers also have proposed special processes such as folding [22] and stacking [36] for laser cutting assemblies. LamiFold [19] presents a workflow to fabricate various mechanisms by stacking and gluing laser-cut sheets. Special patterns have also been proposed to form meta-materials to approximate volumetric shapes [34]. Kirigami Haptic Swatches [6] create different button-press sensations using cut-and-fold techniques such as kirigami and origami. Several techniques such as strained joint that uses surrogate folds [11] have been proposed to make rigidly foldable origami using non-compliant materials that have thickness [17]. Many approaches such as using wood stripes [24], ribbon fabrics [31], thin spirals [39] and auxetics [15, 16] have been used to compose 3D surfaces.

To summarize, in contrast to the aforementioned works, our work discovers laser-cut joinery and formulates a fabrication-aware method with a computational model for creating 3D objects by

directly unfolding the 3D model to a 2D plan and folding the cut-in-place pieces back to articulated angles on one sheet of material. Specifically, our method (1) has no extra computational model to convert 3D models to 2D cutting plans, (2) requires only one sheet of material without stacking and heating, and (3) largely simplifies the post-fabrication and assembling process by making pieces folding in place in almost arbitrary angle compared to previous laser cutting methods.

### 3 T-PATTERN GEOMETRY

Our method rests on the key contribution of 2 T-pattern geometries that enable 2 cut-in-place pieces to be constrained at an angle when folding inward ( $<\theta$ -T-pattern) and outward ( $>\theta$ -T-pattern) as shown in Figure 2. In this section, we derive their parametric models from the illustration of the T-pattern geometries as shown in Figure 5 respectively to predict the articulated angle and describe how they accommodate articulated joints and detent hinges as shown in Figure 3.

In short, the T-pattern creates a rotary latch at an articulated angle. The key factors in determining the articulated angle  $\theta$  are the thickness  $T$  of the board, the neck length  $L$  of the pattern, and the base displacement  $X$  relative to the shared pivot edge.

Figure 5a,b depict the geometries of  $<\theta$ -T-pattern in the cases of an acute and an obtuse angle respectively, which gives the following equation:

$$X \cos \theta + T \sin \theta = L \quad (1)$$

Figure 5c,d depict the geometries of  $>\theta$ -T-pattern in the cases of an acute and an obtuse angle respectively, which gives the following equation:

$$\begin{cases} L = |T \csc \theta| & \text{for } \theta \leq 90^\circ \\ L = |T \csc \theta| - X_{ext} \tan \theta & \text{for } \theta > 90^\circ \end{cases} \text{ and } X = T \cot \theta + X_{ext} \quad (2)$$

We should note that  $T$  and  $L$  are positive values, while the value of  $X$  can be either positive or negative, meaning the direction of the base displacement.  $X_{ext}$  is the key factor that influences the holding force of detent hinges and can be fine-tuned in our user interface.

Moreover, the laser cutting kerf [35], i.e., the uneven burned materials at the top and the bottom in the laser-cutting process as shown in Figure 6, causes a position offset  $K$  and an angular offset  $\alpha$ . To compensate for the angular offset  $\alpha$ , equation 1 is further modified into:

$$X \cos(\theta + \alpha) + T \sin(\theta + \alpha) = L \cos \alpha + T \sin \alpha \quad (3)$$

while in equation 2  $\theta$  is substituted by  $\theta + \alpha$ . Finally, we add extra corrections to compensate for the position offset  $K$  and the folding direction (mountain or valley) to obtain the final value  $L_c$  and  $X_c$ . The correction detail is shown in Table A.1 of appendix A.

#### 3.1 Determining Parameters

In practice, we designate the thickness  $T$  and the articulated angle  $\theta$ . We also assume that the kerf position offset  $K$  and the angular offset  $\alpha$  remain constant anywhere on the cutting board. That is, the neck length  $L$  and the base displacement  $X$  are the two parameters that have to be determined.

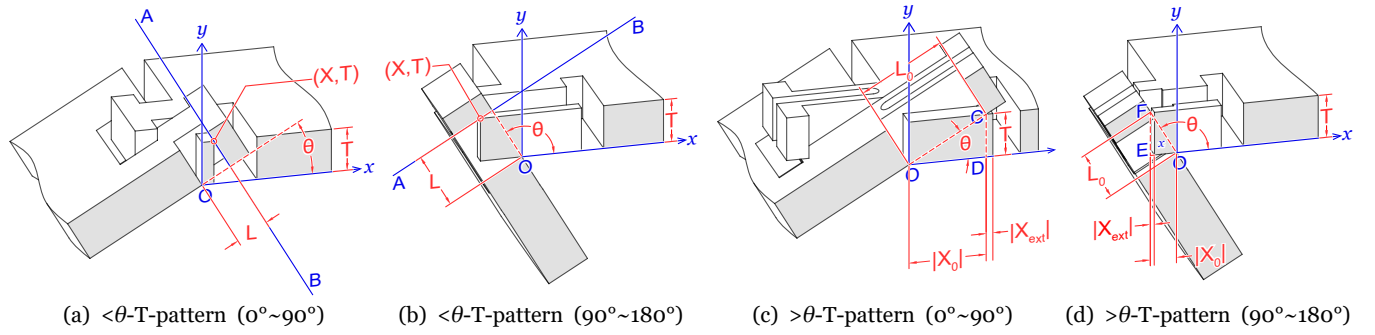


**Figure 5: The cross-sectional geometries of the 2 types of T-pattern in 2 folding ranges. For  $\lt;theta</math>-T-patterns in (a) and (b), we assume that the two boards are folded perfectly along the shared edge and thus set the pivot point as the origin  $O$  of the coordinate system with the  $x$  axis pointing away horizontally and the  $y$  axis pointing away vertically. At the moment when the two boards are at the articulated angle  $\theta$ , the head segment of the left board contacts the base segment of the right board, i.e.,  $\overline{AB}$  intersects the point  $(X, T)$ , and thus prevents folding more. Since the length of the perpendicular from the origin  $O$  to  $\overline{AB}$  is exactly  $L$  and the angle the perpendicular makes to the positive direction of the  $x$ -axis is  $\theta$ ,  $\overline{AB}$  can be described in the normal form as equation 1. For  $\lt;theta</math>-T-patterns in (c) and (d), they incorporate a cantilever beam to form a ratchet at the head segment. The head segment deforms as the folding angle of the two boards approaches  $\theta$  and then snaps at the angle  $\theta$ , which then prevents them from being folded back to the flat position. The contact point of the head segment forms a right triangle ( $\triangle OCD$  or  $\triangle OFE$ ) with the pivot. This gives the equations  $L_0 = |T \csc \theta|$  and  $X_0 = T \cot \theta$ . However, the head segment only touches at a point ( $C$  or  $F$ ) without snapping. To make the head segment collide and snap, we extend the base segment by  $X_{ext}$  for angles  $0^\circ \sim 90^\circ$  in (c) and shorten the base segment by  $X_{ext}$  for angles  $90^\circ \sim 180^\circ$  in (d). Equation 2 includes this adjustment and describes  $X$  and  $L$  that we use to provide proper contact and achieve the desired holding force.$$**

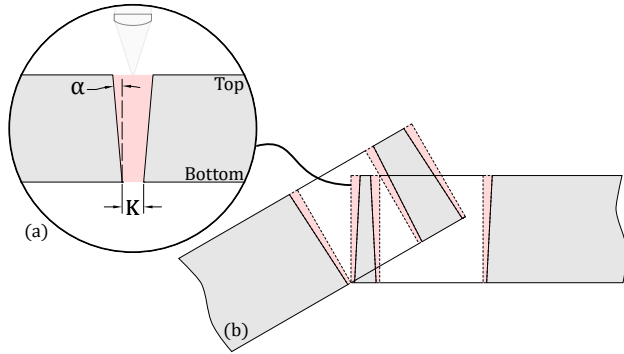


**Figure 6: The laser cutting kerf affects the geometry in Flaticulation. (a) We define the position offset  $K$  and the angle offset  $\alpha$  to describing the kerf. (b) The cross-sectional view of the offset effect. Specifically, the kerf causes the contact points of the boards to shift on the actual cut and induces additional rotation. In the meantime, since the width of the kerf at the top and the bottom differs, mountain folds (convex) and valley folds (concave) cause different errors that need to be considered separately.**

It is trivial for  $\gt;theta</math>-T-pattern to get the exact pair of  $L$  and  $X$  by solving equation 2. More specifically, we set  $X_{ext}$  to be  $0.3T \sin \theta$ , which worked the best for MDF and acrylic sheets from our empirical testing.$

However, for  $\lt;theta</math>-T-pattern there are multiple solutions when solving equation 3. Figure A.1a of appendix A plots the solution$

space of equation 3 with regard to  $L$ ,  $X$  and  $\theta$ . As shown in the plot, there are multiple combinations of  $L$  and  $X$  that achieve the same angle (with the same color code on the curved surface).

In our implementation, we focus on reducing the size of the pattern and find that the additional relation between  $L$  and  $X$  shown in equation 4 works out the best to determine their values.

$$X = \begin{cases} T - L & \text{for } \theta \leq 90^\circ \\ -L & \text{for } \theta > 90^\circ \end{cases} \quad (4)$$

From this parametric model, we find that large angles ( $\theta > 150^\circ$ ) require a very long neck. In addition, the kerf makes small folding angles ( $\theta < 7^\circ$ ) unachievable with our laser cutter. Figure A.1b of appendix A shows our achieved angles  $\theta$  relative to  $L$  under equation 3 and 4 with  $T = 3$  mm,  $K = 0.12$  mm and  $\alpha = 2.1^\circ$  for  $\lt;theta</math>-T-pattern.$

### 3.2 Articulated Joints

We achieve articulated joints that interlock at desired angles by lining  $\lt;theta</math>-T-pattern and  $\gt;theta</math>-T-pattern on a single edge. The  $\lt;theta</math>-T-patterns stops the boards from further folding and the  $\gt;theta</math>-T-patterns prevent it from going back to the flatten position, achieving torque equilibrium.$$$$

For joints with  $\theta$  in the range  $0^\circ \sim 90^\circ$ , the 2 types of T-patterns combined interlock the two pieces together, achieving force equilibrium, as shown in Figure A.1c of appendix A. All 6 degrees of freedom are consequently constrained, forming joints at the articulated angle.

Joints with  $\theta$  in the range of  $90^\circ \sim 180^\circ$ , however, lack the holding force from downward, thus requiring an extra lattice hinge to be added along the edge to form the joint. The lattice hinge provides the

force needed to hold the two pieces together while the T-patterns clutches at the articulated angle to achieve torque equilibrium.

### 3.3 Detent Hinges

We achieve detent hinges by combining  $>\theta$ -T-patterns and lattice hinges. The detent is achieved with the cantilever beam working as a ratchet. Figure A.1d of appendix A shows the torque-angle plot of our example detent hinge, where  $\Delta\theta$  is the difference from the initial position. The bump from  $\Delta\theta \sim 3^\circ$  to  $\Delta\theta \sim 10^\circ$  is the detent created by the  $>\theta$ -T-pattern. That is, the user feels the apparent change in resistance when bending the pieces more than the articulated angle. The force of the detent can be adjusted by changing the length of  $X_{ext}$  mentioned in section 3.

## 4 FLATICULATION USER INTERFACE

We provide a software interface for Flaticulation. Our software (1) unfolds 2-manifold models, (2) adds the articulated joints between connecting pieces using the articulated angles in the model, and (3) allows adjusting joint types and parameters for each connection. We implemented the software as a Rhinoceros plugin using Python and Grasshopper. We used Trimesh [9] library for mesh flattening, HumanUI for the interface, and GH\_CPython [1] for integrating Python functions into Grasshopper. Our software is open source and can be found online at <http://flaticulation.com/>.

### 4.1 Unfold 2-Manifold Models

Our software unfolds a 3D model onto a 2D plan to be laser-cut using the strategy proposed by Haenselmann et al. [12]. This method calculates the weights to determine the minimum spanning tree of the mesh's associated graph and thus only supports 2-manifold models, which fits for one of the Flaticulation limitations. In addition, our software records polygons' articulated angles and their folding directions on their connecting edges while executing the unfolding procedure for generating the right articulated joints by default. The user interface for unfolding models, as shown in Figure 4a, provides the options for scaling the original model and designating material thickness  $T$ , kerf offset  $K$ , and kerf angle  $\alpha$  for generation. Our software calculates the corresponding  $L$  and  $X$  based on section 3.1 and repetitively fills the length of the edge with the T-patterns by default.

### 4.2 Add Joints and Hinges

Our software also allows users to manually add joints or hinges with desired settings onto each edge. That is, users can fine-tune the unfolded 2D plan or create their custom 2D plans without building 3D models and apply Flaticulation. The user interface for adding joints, as shown in Figure 7, appears when selecting an edge on the 2D plan and provides the options for changing its joint types (joint or detent hinge), articulated angle, and folding directions. We also include advanced options such as the percentage of length used for adding patterns, the width of small 'tab' [35] that prevents fabricated objects from falling out while easy to break by folding, and the stiffness of the hinge.

For detent hinges, there are more options for creating a normal hinge and detent mechanism with and without a stopping angle. As described in section 3.3, modifying the length of the parameter

$X_{ext}$  results in changes in the detent resistance. We, therefore, use a multiplier of  $X_{ext}$  (from 0 to 1, 0.5 by default) to specify the stiffness of the detent. The higher the stiffness the more rigid the detent becomes. Additionally, users can set the stopping angle to the detent hinge, where an  $<\theta$ -T-pattern is added to limit the range the hinge can work at.

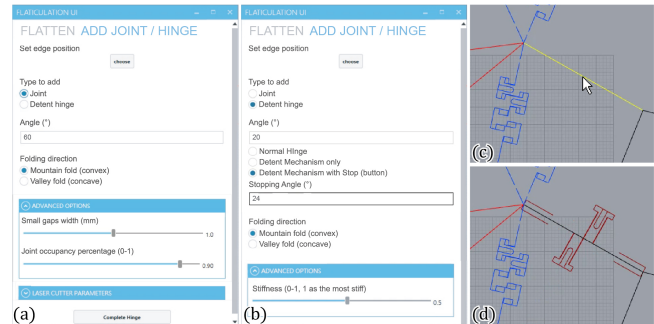


**Figure 7: The Flaticulation user interface allows users to add individual (a) articulated joints or (b) detent hinges besides generating joints from 3D models automatically. (c) Users can select a line segment at the desired location, (d) then the corresponding pattern will be generated on the edge according to the settings menu.**

## 5 TECHNICAL EVALUATIONS

We conducted technical evaluations to gain deeper insight for practical use of Flaticulation. In particular, we evaluated the error of the articulated angle and the strength of the articulated joints in the following section.

### 5.1 Angular Error

To validate our parametric model of the articulated angles achieved by the T-patterns in section 3, we cut 20 samples of a joint that was designed to clutch at an angle and measured its actual clutched angle. We photographed the joint horizontally using a telephoto lens (35mm-Equivalent 216 mm) from their side and then measured the angles digitally by putting the image in AutoCAD. We tested 5 different angles ( $30^\circ$ ,  $60^\circ$ ,  $90^\circ$ ,  $120^\circ$ ,  $150^\circ$ ) with total 100 samples. Figure 8 shows more details of the joint samples in the 5 articulated angles. The fabricated 100 samples have an average error of  $-3.21^\circ$ .

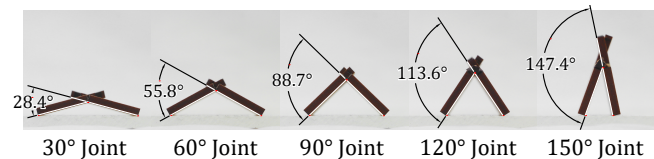


**Figure 8: The joint samples in  $30^\circ$ ,  $60^\circ$ ,  $90^\circ$ ,  $120^\circ$  and  $150^\circ$ . The respective min-max pairs are  $[26.1^\circ, 29.9^\circ]$ ,  $[49.4^\circ, 65.5^\circ]$ ,  $[84.7^\circ, 91.8^\circ]$ ,  $[111.7^\circ, 114.9^\circ]$  and  $[144.6^\circ, 149.0^\circ]$ . The respective mean errors are  $-1.56^\circ$ ,  $-4.17^\circ$ ,  $-1.28^\circ$ ,  $-6.42^\circ$  and  $-2.64^\circ$  ( $SD = 1.12, 4.83, 2.14, 0.73, 1.36$ ).**

## 5.2 Structural Strength

To evaluate the strength of the joints and gain more insight to strengthen the joints, we first performed simulations using the finite element method to understand the structure, then conducted a stress-strain analysis using a tensile testing machine.

**5.2.1 Simulation.** We used Fusion 360 for the finite element analysis. The simulation was set up by fixing one board by the edge and applying a perpendicular load of 0.5 N on the other board with a distance to the axis of 2 cm, creating a 1 N · cm torque. Figure 9 shows the simulation result of the stress distribution. As shown in Figure 9a,c, the stress is concentrated at the base of the  $<\theta$ -T-pattern when being pushed down while being concentrated near the neck of the  $>\theta$ -T-pattern when being pulled up, which matches the actual point of failure as shown in Figure 9b,d. These are locations that should be reinforced if a stronger joint is needed.

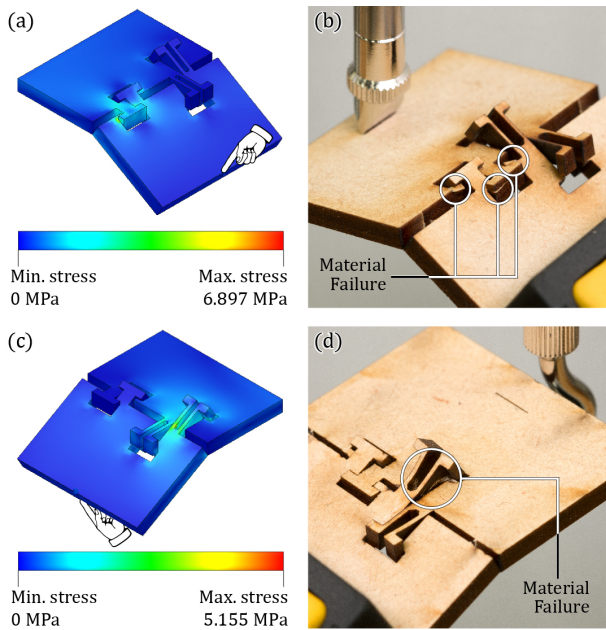


**Figure 9:** The results of the stress distribution in our finite element analysis and the actual points of failure under pushing (a,b) and pulling force (c,d).

We also compared the structural strength under different material thicknesses and different widths of the T-patterns using the finite element method. We ran simulations using (1) the material thickness ranging from 3 mm to 12 mm with the width fixed at 6 mm and (2) the width of individual T-pattern ranging from 6 mm to 24 mm with the thickness fixed at 3 mm. The load applied remains the same, creating a 1 N · cm torque. Their corresponding maximum stress in the structure is plotted in Figure 10. Our results show that the maximum stress in the structure decreases as the material becomes thicker or the width of the pattern increases, indicating increasing structural strength and better distribution of the stress. We did not test the interaction between the material thickness and the pattern’s width. We should note that the spike when pushing around 12 mm in Figure 10b is the correct simulation result from

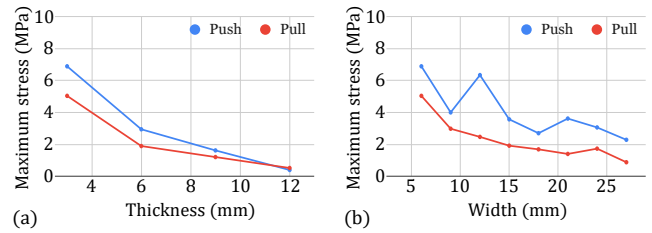


**Figure 10:** The maximum stress in the simulated structure of the articulated joint decreases as (a) material thickness increases or (b) width of the T-pattern increases.

Fusion 360. We suspected that the spike to be an exception in the finite element analysis in Fusion 360 or the interaction of the certain thickness.

**5.2.2 Tensile Testing.** We conducted the stress-strain analysis with our computer-control tensile testing machine, shown in Figure 11. The test piece is mounted on a multi-angle vise with one board leveled. The load cell pushes/pulls against the test piece at a fixed distance from the rotating axis (20 mm for pushing; 35 mm for pulling) and lowers/rises at a rate of 1 mm/min. The force and the time were recorded on the computer with a sampling rate of 3.4 Hz. The distance for each data point was calculated from the time and the final position measured from the caliper.

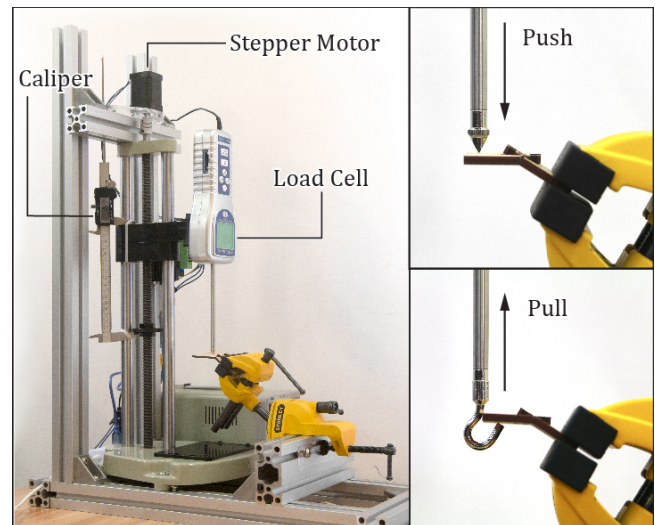


**Figure 11:** Stress-strain analysis apparatus. A load cell and a caliper were mounted on a motorized tensile testing machine. A multi-angle vise clamps the test piece so that the articulated joint is pushed/pulled perpendicularly.

We tested articulated joints on 3 mm thick acrylic at 60°, and on 3 mm thick MDF with angles ranging from 10° to 160° with 10° interval. Each joint was sampled twice: being pushed and being pulled. Joints with articulated angles  $< 7^\circ$  cannot be achieved due to the laser-cut kerf, and joint with articulated angles  $> 160^\circ$  requires a very long neck, thus they were left out.

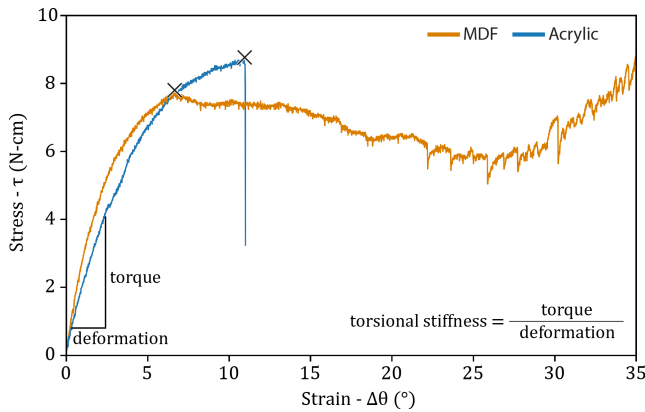
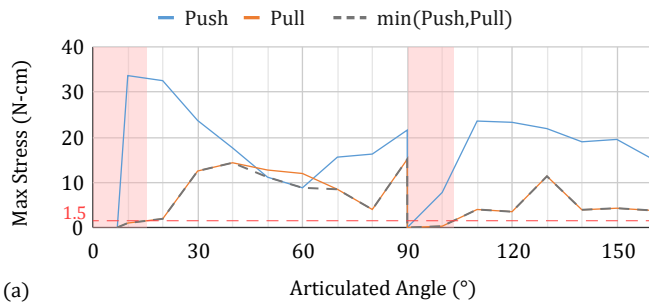


**Figure 12: Stress-strain curves of articulated joints with MDF and acrylic as the material.**

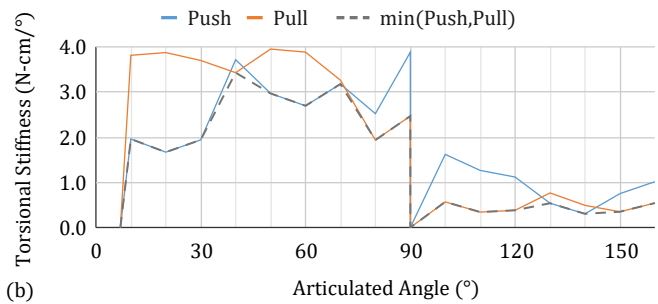
We analyzed the stress-strain curves of the articulated joints among different angles by focusing on 2 characteristics: (1) the maximum stress and (2) the torsional stiffness. We measured the maximum stress by recording the maximum reading of the load cell until the test piece broke up or deformed over 40°. We derived the torsional stiffness using the current torque over the current deformation angle measured on the tensile testing machine. An ideal joint should have high maximum stress and high stiffness both during pushing and pulling.

Figure 12 shows the stress-strain curves of 60° articulated joints of MDF and acrylic under pushing force. The linear part of the stress-strain curve suggests the joint is in the elastic deformation initially for both MDF and acrylic. The sudden drop marked × indicates the crack point. Acrylic appears to withstand a higher load before starting to break. Although acrylic breaks at a higher load, its brittle nature makes the articulated joint fail completely after reaching that point. MDF on the other hand holds together after the initial crack but becomes unstable afterward.

Figure 13 shows (a) the maximum stress and (b) the torsional stiffness over a range of angles using MDF. We also highlighted the overall minimum value among pushing and pulling using a dashed line. The strength of the 40° articulated joint is the highest which has the highest minimum value in both the maximum stress and the torsional stiffness. We also found that the stiffness of joints



(a)



(b)

**Figure 13: (a) Maximum withstanding stress measured among joints with different articulated angles; joints should withstand at least 1.5 N-cm of torque. (b) Torsional stiffness among joints with different articulated angles.**

with angles less than 90° is generally higher than joints with angles greater than 90°. From our empirical testing, we found that joints should withstand at least 1.5 N-cm to be useful in practice. Joints with angles less than 15° and from 90° to 103° fall below this region, which are indicated by the red boxes in Figure 13a.

### 5.3 Summary

To sum up our evaluation results on MDF, we found that (1) the articulated joint has an average of -3.21° angular error to its articulated angle; (2) the thicker the material or the wider the T-pattern, the stronger the articulated joint; (3) acrylic is stronger while MDF sustains better; (4) articulated joints at different angles have different strengths and could bear up to 34 N-cm of torque and 4 N-cm/° torsional stiffness; (5) the 40° articulated joint has the highest minimum value in both the maximum stress and the torsional stiffness; (6) the joints with articulated angles from 0° to 15° and from 90° to 103° do not have sufficient strength and should not be used.

## 6 FLATICULATION OBJECTS

As shown in Figure 1, we made several objects to validate Flaticulation and demonstrate its potential. The objects can be broadly categorized into (1) 2-manifold models whose laser-cut plans are generated from their 3D models by our software, (2) non-manifold models whose laser-cut plans are crafted using our software, and (3) functional objects with and without mechanisms. We show selected functional objects in Figure 14 and put more details of all objects we made in appendix B.

We made each of the 2-manifold models shown in Figure B.1 from a 3D model. We used our Flaticulation software to unfold the 3D model into a 2D plan with the articulated joints automatically added according to the articulated angles on each of the edges. As our current software does not handle overlapping pieces while unfolding, we manually partitioned the overlapping parts in the 2D laser-cut plan or in the 3D model. In particular, the wolf had its 2D laser-cut plan manually partitioned since it had 3 overlapping pieces after unfolding. The bunny, on the other hand, was done by partitioning the 3D model into 6 parts before importing it into our software to generate the laser-cut plan without overlapping pieces. We combined the 6 unfolded plans and manually added connecting joints between them.

Non-manifold models shown in Figure B.3 resemble origami models that cannot be unfolded using their 3D models. We made

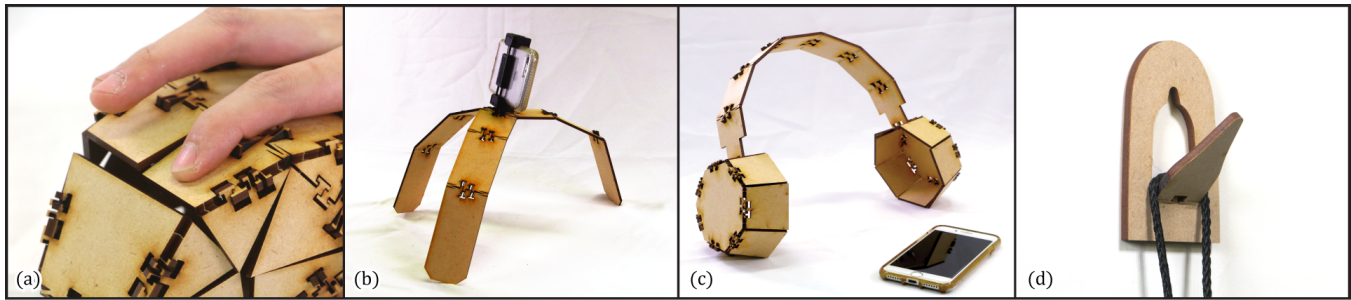


**Figure 14: Selected functional objects fabricated with Flaticulation. From left to right: computer mouse with buttons that click; an adjustable tripod; a headphone with a headband that can be tightened; a hook that can be folded flat when not in use.**

these objects by directly sketching their 2D plan using our Flaticulation software to add individual articulated joints. The outline of each piece as well as the articulated angle on the connecting edge were determined during our design process.

The mouse shown in Figure 14a uses our detent hinges to demonstrate clicking. We (1) modeled the mouse hull in a 3D modeling software, (2) unfolded the model in our user interface, (3) added the detent hinges on the unfolded 2D plan, and then fabricated it. We manually added the detent hinge on the 2D plan to avoid the software wrongly unfolding the button part. We also ensured that the other sides of the button part were completely cut off so that the detent hinge was the only connecting edge.

We made our headphones (Figure 14c) and tripod (Figure 14b) to demonstrate reconfigurable objects using our multi-stable articulated hinge. By lining multiple detent hinges with different detent angles, the headband can be loosened or tightened by bending it to different angles. The same as for the tripod. With each hinge having 2 stable angles, the entire structure can be fixed on multiple different configurations. We sketched the reconfigurable parts directly from scratch on a blank 2D plan and added articulated hinges, then joined them with the static parts (earcups) unfolded from 3D models.

Finally, by utilizing the  $<\theta$ -T-pattern along with a lattice living hinge, the  $<\theta$ -T-pattern limits the swinging motion, resulting in a simple foldable hook (Figure 14d). The hook is capable of hanging more than 1 kg of weight. While we did not conduct a stress test on the reversibility of the hinge, the hook could be folded back flat and even bent over to the other side to a different angle.

To give an idea of the time to fabricate the models, we take our mouse as an example and give our rough timing measurements. Having 28 individual pieces, modeling took about 2 minutes (converting from a 3D model and creating the button mechanism), laser cutting took 7 minutes, and assembling took about 2 minutes.

## 7 DISCUSSION

Through our initial discovery, geometric analysis, software development, technical evaluations, and building real objects, we have gained a deeper understanding of the working principles and limitations of our proposed method. While Flaticulation has not yet achieved fabricating arbitrary 3D objects by 2D laser cutting their unfolded 3D meshes, it takes a key step by enabling two cut-in-place pieces to be joined at an articulated angle. In this section, we

discuss challenges with regard to building a more robust Flaticulation system to enlighten the future space of 3D laser cut objects and acknowledge potential failures in broader uses.

### 7.1 Mechanically Stabilized Unfolding

The current unfolding algorithm optimizes for the least number of overlapping pieces and disregards other Flaticulation properties especially joint strength and error. By introducing our results of joint strength and error as the new constraints, the unfolding algorithm could play an important role in generating mechanically stabilized Flaticulation objects. For example, since the  $40^\circ$  articulated joint has the highest strength, the 3D model can be remeshed with the highest weight on  $40^\circ$  articulated polygons. The gravitational force should also be considered in the unfolding algorithm to achieve a better mechanically stabilized structure. Integrating other joints during unfolding, such as adding finger joints on edges that do not have Flaticulation joints, could also stabilize the entire structure. This can be done by adjusting the weighting of the mesh's associated graph accordingly when computing the minimal spanning tree in the unfolding algorithm to decide the joints to be used.

### 7.2 Optimizing Repetition and Size

From our observations during the strength evaluation, we also noticed that having repeating patterns on an edge increases the strength and stiffness of the joint. That is, edge length also plays a role in the strength of the joints as the wider the T-pattern or the more repeating patterns along an edge, the stronger the joint is. However, we made several attempts to conduct FEA on multiple joints in Fusion 360 but did not get a successful pass yet. The interaction of our joints seems to crash the simulation process. More investigation is needed to figure out the correlation between the number of repeating patterns and the width of the pattern to optimize the size of the joint.

We also noticed that the head segments on the two sides of the  $<\theta$ -T-pattern do not have the same strength. Specifically shown in Figure 15, location (a) is much weaker than location (b), especially when  $|X|$  is small, i.e. joints with angles close to  $90^\circ$ .

By remixing the pattern, only keeping the 2 middle parts of the  $<\theta$ -T-pattern and replacing the outsides with  $>\theta$ -T-pattern, as shown in the right of Figure 15, the new articulated joint pattern could be stronger and more space-efficient.

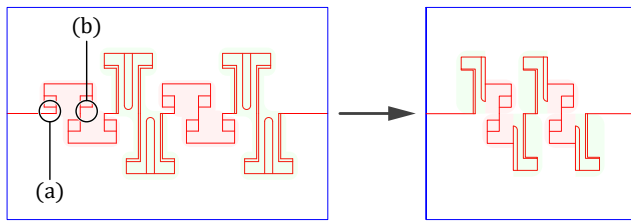


**Figure 15: A stronger joint with a smaller profile might be possible by rearranging the two T-patterns.**

Our preliminary tests show that the new pattern arrangement has similar strength while occupying less space, which allows more repetition on edges of the same length, resulting in stronger joints. With a smaller yet stronger joint, the assembled structure would have better structural strength, giving users more freedom while using Flaticulation.

### 7.3 Sorting Assembly Sequence

The models can be assembled by folding the joints in any order most of the time. However, obstruction between the boards occurs once in a while when fabricating non-convex shapes. Users should be able to solve them intuitively by reversing a few steps (folds) for most cases, as shown in Figure 16.

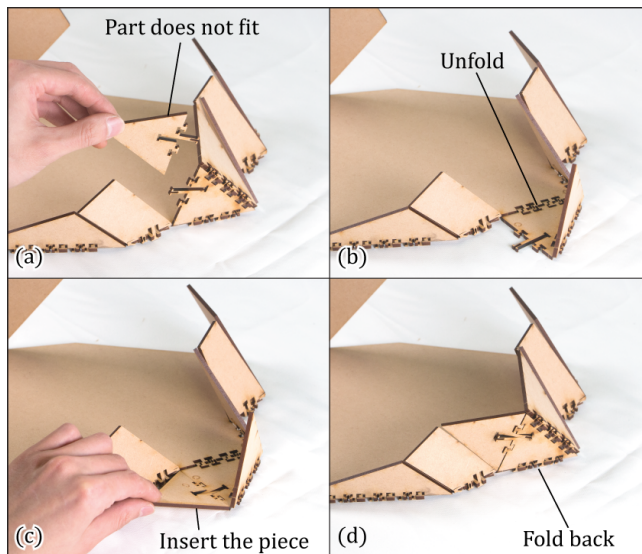


**Figure 16: The process of assembling parts that are blocked due to assembly sequence: (a) The part does not have enough clearance to be assembled due to assembly sequence. (b) Reverse the assembly by unfolding an articulated joint. (c) The part that could not fit previously can then be placed horizontally and folded to be assembled. (d) Finally, the reversed step is folded back.**

To further assist users with this problem, additional features need to be added to the software. First, the locations where the folding sequence must be considered need to be identified; this

can be achieved by simulating the assembly process and detecting interference when folding. After being detected, a quick search among different folding sequences should show a feasible folding sequence to assemble boards. Finally, instructions for the feasible folding sequence would be laser engraved onto the pieces to guide users.

### 7.4 Computer-facilitated 2D Planning

The current software for the Flaticulation user interface cannot handle overlapping pieces automatically, which then requires manual partitioning of the 2D laser-cut plan or 3D model. Computer-facilitated planning should be incorporated into the user interface to suggest potential manual intervention so the workflow becomes easier for users. Besides partitioning pieces to avoid overlaps, more recommendations for creating a Flaticulation 2D plan from scratch could also be possible by borrowing folding principles from origami.

### 7.5 Material Wear-off and Robustness

We should note that a more thorough evaluation regarding the structural strength of the entire Flaticulation object is required, especially those functional objects, to ensure their robustness. Since Flaticulation joints must be clutched together, the linkage between each piece has to be acyclic (tree structure), making each articulated joint crucial when holding the entire structure. The overall structure could be weaker because of the accumulating weights and poorly chosen articulated joint edge, which become breakpoints in the fabricated model.

Material wear-off is also a concern. By close inspection, the head and base segment of the T-patterns, especially the  $>\theta$ -T-pattern, shows slight wear-off after multiple cycles of clutching and unclutching the articulated joints. This is also observed in the mechanisms of detent hinges. This does not affect static objects which are assembled once. The wear-off, nonetheless, affects functional objects. A complete investigation on the robustness of articulated joint and detent hinge due to material wear-off is needed to have long-lasting Flaticulation objects.

## 8 CONCLUSION

We have presented Flaticulation, a method to laser cut joints that makes two cut-in-place flat boards clutch at articulated angles. We have walked through our systematic development from our core discovery—the 2 types of T-patterns to our fabrication-aware editor for Flaticulation. We also have conducted a series of validations including tensile testing and building actual objects. With Flaticulation, we enable a more elegant way to fast assemble 3D polygon models and detent mechanisms using one sheet of 2D laser cut board. We see Flaticulation has a great potential to be broadly used in creating 3D laser cut objects and computational origami.

## ACKNOWLEDGMENTS

This work was supported by the Ministry of Science and Technology in Taiwan (MOST 111-2636-E-002-021).

## REFERENCES

- [1] Mahmoud AbdelRahman. 2017. *GH\_CPython: Alpha release of GH\_CPython plugin*. <https://doi.org/10.5281/zenodo.888148>

- [2] Muhammad Abdullah, Romeo Sommerfeld, Laurenz Seidel, Jonas Noack, Ran Zhang, Thijs Roumen, and Patrick Baudisch. 2021. Roadkill: Nesting Laser-Cut Objects for Fast Assembly. In *The 34th Annual ACM Symposium on User Interface Software and Technology* (Virtual Event, USA) (UIST '21). Association for Computing Machinery, New York, NY, USA, 972–984. <https://doi.org/10.1145/3472749.3474799>
- [3] Patrick Baudisch, Arthur Silber, Yannis Kommanna, Milan Gruner, Ludwig Wall, Kevin Reuss, Lukas Heilman, Robert Kovacs, Daniel Rechlitz, and Thijs Roumen. 2019. *Kyub: A 3D Editor for Modeling Sturdy Laser-Cut Objects*. Association for Computing Machinery, New York, NY, USA, 1–12. <https://doi.org/10.1145/3290605.3300796>
- [4] Dustin Beyer, Serafima Gurevich, Stefanie Mueller, Hsiang-Ting Chen, and Patrick Baudisch. 2015. Platener: Low-Fidelity Fabrication of 3D Objects by Substituting 3D Print with Laser-Cut Plates. In *Proceedings of the 33rd Annual ACM Conference on Human Factors in Computing Systems* (Seoul, Republic of Korea) (CHI '15). Association for Computing Machinery, New York, NY, USA, 1799–1806. <https://doi.org/10.1145/2702123.2702225>
- [5] Ruei-Che Chang, Chih-An Tsao, Fang-Ying Liao, Seraphina Yong Yong, Tom Yeh, and Bing-Yu Chen. 2021. Daedalus in the Dark: Designing for Non-Visual Accessible Construction of Laser-Cut Architecture. In *Proceedings of the 34th Annual ACM Symposium on User Interface Software and Technology* (Virtual Event, USA) (UIST '21). Association for Computing Machinery, New York, NY, USA, 15. <https://doi.org/10.1145/3472749.3474754>
- [6] Zekun Chang, Tung D. Ta, Koya Narumi, Heeju Kim, Fuminori Okuya, Dongchi Li, Kunihiro Kato, Jie Qi, Yoshinobu Miyamoto, Kazuya Saito, and Yoshihiro Kawahara. 2020. *Kirigami Haptic Swatches: Design Methods for Cut-and-Fold Haptic Feedback Mechanisms*. Association for Computing Machinery, New York, NY, USA, 1–12. <https://doi.org/10.1145/3313831.3376655>
- [7] Desai Chen, Pitchaya Sitthi-amorn, Justin T. Lan, and Wojciech Matusik. 2013. Computing and Fabricating Multiplanar Models. *Computer Graphics Forum* 32, 2pt3 (2013), 305–315. <https://doi.org/10.1111/cgf.12050> arXiv:<https://onlinelibrary.wiley.com/doi/pdf/10.1111/cgf.12050>
- [8] Paolo Cignoni, Nico Pietroni, Luigi Malomo, and Roberto Scopigno. 2014. Field-Aligned Mesh Joinery. *ACM Trans. Graph.* 33, 1, Article 11 (Feb. 2014), 12 pages. <https://doi.org/10.1145/2537852>
- [9] Dawson-Haggerty et al. [n.d.]. *trimesh*. <https://trimsh.org/>
- [10] R.J. DeCristoforo. 1997. *The Complete Book of Wood Joinery*. Sterling Publishing Company. <https://books.google.com.tw/books?id=wORfNQAACAAJ>
- [11] Isaac L. Delimont, Spencer P. Magleby, and Larry L. Howell. 2015. A Family of Dual-Segment Compliant Joints Suitable for Use as Surrogate Folds. *Journal of Mechanical Design* 137, 9 (07 2015). <https://doi.org/10.1115/1.4030875> arXiv:[https://asmedigitalcollection.asme.org/mechanicaldesign/article-pdf/137/9/092302/6227543/md\\_137\\_09\\_092302.pdf](https://asmedigitalcollection.asme.org/mechanicaldesign/article-pdf/137/9/092302/6227543/md_137_09_092302.pdf) 092302.
- [12] Thomas Haenselmann and Wolfgang Effelsberg. 2012. Optimal strategies for creating paper models from 3D objects. *Multimedia systems* 18, 6 (2012), 519–532.
- [13] Kristian Hildebrand, Bernd Bickel, and Marc Alexa. 2012. crdbrd: Shape Fabrication by Sliding Planar Slices. *Computer Graphics Forum* 31, 2pt3 (2012), 583–592. <https://doi.org/10.1111/j.1467-8659.2012.03037.x> arXiv:<https://onlinelibrary.wiley.com/doi/pdf/10.1111/j.1467-8659.2012.03037.x>
- [14] Jerzy Jasięko, Tomasz Nowak, and Anna Karolak. 2014. Historical carpentry joints. *Wiadomości Konserwatorskie - Journal of Heritage Conservation* 40 (12 2014), 58–82.
- [15] Mina Konaković, Keenan Crane, Bailin Deng, Sofien Bouaziz, Daniel Piker, and Mark Pauly. 2016. Beyond Developable: Computational Design and Fabrication with Auxetic Materials. *ACM Trans. Graph.* 35, 4, Article 89 (July 2016), 11 pages. <https://doi.org/10.1145/2897824.2925944>
- [16] Mina Konaković-Luković, Julian Panetta, Keenan Crane, and Mark Pauly. 2018. Rapid Deployment of Curved Surfaces via Programmable Auxetics. *ACM Trans. Graph.* 37, 4, Article 106 (July 2018), 13 pages. <https://doi.org/10.1145/3197517.3201373>
- [17] Robert J. Lang, Kyler A. Tolman, Erica B. Crampton, Spencer P. Magleby, and Larry L. Howell. 2018. A Review of Thickness-Accommodation Techniques in Origami-Inspired Engineering. *Applied Mechanics Reviews* 70, 1 (02 2018). <https://doi.org/10.1115/1.4039314> arXiv:[https://asmedigitalcollection.asme.org/appliedmechanicsreviews/article-pdf/70/1/010805/5964551/amr\\_070\\_01\\_010805.pdf](https://asmedigitalcollection.asme.org/appliedmechanicsreviews/article-pdf/70/1/010805/5964551/amr_070_01_010805.pdf) 010805.
- [18] Maria Larsson, Hironori Yoshida, Nobuyuki Umetani, and Takeo Igarashi. 2020. *Tsugite: Interactive Design and Fabrication of Wood Joints*. Association for Computing Machinery, New York, NY, USA, 317–327. <https://doi.org/10.1145/3379337.3415899>
- [19] Danny Leen, Nadya Peek, and Raf Ramakers. 2020. LamiFold: Fabricating Objects with Integrated Mechanisms Using a Laser Cutter Lamination Workflow. In *Proceedings of the 33rd Annual ACM Symposium on User Interface Software and Technology* (Virtual Event, USA) (UIST '20). Association for Computing Machinery, New York, NY, USA, 304–316. <https://doi.org/10.1145/3379337.3415885>
- [20] Shiran Magrisso, Moran Mizrahi, and Amit Zoran. 2018. Digital Joinery For Hybrid Carpentry. In *Proceedings of the 2018 CHI Conference on Human Factors in Computing Systems* (Montreal QC, Canada) (CHI '18). Association for Computing Machinery, New York, NY, USA, 1–11. <https://doi.org/10.1145/3173574.3173741>
- [21] James McCrae, Nobuyuki Umetani, and Karan Singh. 2014. FlatFitFab: Interactive Modeling with Planar Sections. In *Proceedings of the 27th Annual ACM Symposium on User Interface Software and Technology* (Honolulu, Hawaii, USA) (UIST '14). Association for Computing Machinery, New York, NY, USA, 13–22. <https://doi.org/10.1145/2642918.2647388>
- [22] Stefanie Mueller, Bastian Kruck, and Patrick Baudisch. 2013. LaserOrigami: Laser-Cutting 3D Objects. In *Proceedings of the SIGCHI Conference on Human Factors in Computing Systems* (Paris, France) (CHI '13). Association for Computing Machinery, New York, NY, USA, 2585–2592. <https://doi.org/10.1145/2470654.2481358>
- [23] T. Noll. 2002. *The Joint Book: The Complete Guide to Wood Joinery*. Popular Woodworking Books. <https://books.google.com.tw/books?id=Z7zZAAAAMAAJ>
- [24] Stefan Pillwein, Kurt Leimer, Michael Birsak, and Przemyslaw Musialski. 2020. On Elastic Geodesic Grids and Their Planar to Spatial Deployment. *ACM Trans. Graph.* 39, 4, Article 125 (July 2020), 12 pages. <https://doi.org/10.1145/3386569.3392490>
- [25] G. Rogowski. 2002. *The Complete Illustrated Guide to Joinery*. Taunton Press. [https://books.google.com.tw/books?id=W\\_1TAAAAMAAJ](https://books.google.com.tw/books?id=W_1TAAAAMAAJ)
- [26] Thijs Roumen, Ingo Apel, Jotaro Shigeyama, Abdullah Muhammad, and Patrick Baudisch. 2020. Kerf-Canceling Mechanisms: Making Laser-Cut Mechanisms Operate across Different Laser Cutters. Association for Computing Machinery, New York, NY, USA, 293–303. <https://doi.org/10.1145/3379337.3415895>
- [27] Thijs Roumen, Yannis Kommanna, Ingo Apel, Conrad Lempert, Markus Brand, Erik Brendel, Laurenz Seidel, Lukas Rambold, Carl Goedecken, Pascal Crenzin, Ben Hurdlehey, Muhammad Abdullah, and Patrick Baudisch. 2021. Assembler3: 3D Reconstruction of Laser-Cut Models. In *Proceedings of the 2021 CHI Conference on Human Factors in Computing Systems* (Yokohama, Japan) (CHI '21). Association for Computing Machinery, New York, NY, USA, Article 672, 11 pages. <https://doi.org/10.1145/3411764.3445453>
- [28] Thijs Roumen, Conrad Lempert, Ingo Apel, Erik Brendel, Markus Brand, Laurenz Seidel, Lukas Rambold, and Patrick Baudisch. 2021. AutoAssembler: Automatic Reconstruction of Laser-Cut 3D Models. In *The 34th Annual ACM Symposium on User Interface Software and Technology* (Virtual Event, USA) (UIST '21). Association for Computing Machinery, New York, NY, USA, 652–662. <https://doi.org/10.1145/3472749.3474776>
- [29] Thijs Roumen, Jotaro Shigeyama, Julius Cosmo Romeo Rudolph, Felix Grzelka, and Patrick Baudisch. 2019. SpringFit: Joints and Mounts That Fabricate on Any Laser Cutter. In *Proceedings of the 32nd Annual ACM Symposium on User Interface Software and Technology* (New Orleans, LA, USA) (UIST '19). Association for Computing Machinery, New York, NY, USA, 727–738. <https://doi.org/10.1145/3332165.3347930>
- [30] Greg Saul, Manfred Lau, Jun Mitani, and Takeo Igarashi. 2010. SketchChair: An All-in-One Chair Design System for End Users. In *Proceedings of the Fifth International Conference on Tangible, Embedded, and Embodied Interaction* (Funchal, Portugal) (TEI '11). Association for Computing Machinery, New York, NY, USA, 73–80. <https://doi.org/10.1145/1935701.1935717>
- [31] Christian Schüller, Roi Poranne, and Olga Sorkine-Hornung. 2018. Shape Representation by Zippables. *ACM Trans. Graph.* 37, 4, Article 78 (July 2018), 13 pages. <https://doi.org/10.1145/3197517.3201347>
- [32] Yuliy Schwartzburg and Mark Pauly. 2013. Fabrication-aware Design with Intersecting Planar Pieces. *Computer Graphics Forum* 32, 2pt3 (2013), 317–326. <https://doi.org/10.1111/cgf.12051> arXiv:<https://onlinelibrary.wiley.com/doi/pdf/10.1111/cgf.12051>
- [33] K. Seike, Y. Yobuco, Y. Yobuco, R.M. Davis, R.B.H. Davis, John Weatherhill (Nowy Jork), and Tankōsha Henshūkyoku. 1977. *The Art of Japanese Joinery*. Shambhala. <https://books.google.com.tw/books?id=kn1oHM4LyG4C>
- [34] Madlaina Signer, Alexandra Ion, and Olga Sorkine-Hornung. 2021. *Developable Metamaterials: Mass-Fabricable Metamaterials by Laser-Cutting Elastic Structures*. Association for Computing Machinery, New York, NY, USA. <https://doi.org/10.1145/3411764.3445666>
- [35] Mike Sinclair. 2015. Laser Cutter Tips and Techniques document. <https://www.microsoft.com/en-us/research/publication/laser-cutter-tips-and-techniques-document/>
- [36] Udayan Umapathi, Hsiang-Ting Chen, Stefanie Mueller, Ludwig Wall, Anna Seufert, and Patrick Baudisch. 2015. LaserStacker: Fabricating 3D Objects by Laser Cutting and Welding. In *Proceedings of the 28th Annual ACM Symposium on User Interface Software & Technology* (Charlotte, NC, USA) (UIST '15). Association for Computing Machinery, New York, NY, USA, 575–582. <https://doi.org/10.1145/2807442.2807512>
- [37] Ziqi Wang, Peng Song, and Mark Pauly. 2018. DESIA: A General Framework for Designing Interlocking Assemblies. *ACM Trans. Graph.* 37, 6, Article 191 (dec 2018), 14 pages. <https://doi.org/10.1145/3272127.3275034>
- [38] Ziqi Wang, Peng Song, and Mark Pauly. 2021. MOCCA: Modeling and Optimizing Cone-Joints for Complex Assemblies. *ACM Trans. Graph.* 40, 4, Article 181 (jul 2021), 14 pages. <https://doi.org/10.1145/3450626.3459680>
- [39] Katja Wolff, Roi Poranne, Oliver Glauser, and Olga Sorkine-Hornung. 2018. Packable Springs. *Computer Graphics Forum* 37, 2 (2018), 251–262. <https://doi.org/10.1111/cgf.13358> arXiv:<https://onlinelibrary.wiley.com/doi/pdf/10.1111/cgf.13358>

- [40] Jiaxian Yao, Danny M. Kaufman, Yotam Gingold, and Maneesh Agrawala. 2017. Interactive Design and Stability Analysis of Decorative Joinery for Furniture. *ACM Trans. Graph.* 36, 2, Article 20 (mar 2017), 16 pages. <https://doi.org/10.1145/3054740>
- [41] Clement Zheng, Ellen Yi-Luen Do, and Jim Budd. 2017. Joinery: Parametric Joint Generation for Laser Cut Assemblies. In *Proceedings of the 2017 ACM SIGCHI Conference on Creativity and Cognition* (Singapore, Singapore) (C&C '17). Association for Computing Machinery, New York, NY, USA, 63–74.

### A IMPLEMENTATION DETAILS

**Table A.1: Kerf correction terms for  $L$  and  $X$  under different folding directions and ranges.**

	Mountain Folds (Convex)		Valley Folds (Concave)	
	$0^\circ \sim 90^\circ$	$90^\circ \sim 180^\circ$	$0^\circ \sim 90^\circ$	$90^\circ \sim 180^\circ$
$<\theta$ -T-pattern	$\begin{cases} L_c = L - K \\ X_c = X + K + T \tan \alpha \end{cases}$	$\begin{cases} L_c = L - K \\ X_c = X + K + T \tan \alpha \end{cases}$	$\begin{cases} L_c = L - K - T \tan \alpha \\ X_c = X + T \tan \alpha \end{cases}$	$\begin{cases} L_c = L - K - T \tan \alpha \\ X_c = X + K + T \tan \alpha \end{cases}$
$>\theta$ -T-pattern	$\begin{cases} L_c = L - K \\ X_c = X + T \tan \alpha \end{cases}$	$\begin{cases} L_c = L - K \\ X_c = X + K - T \tan \alpha \end{cases}$	$\begin{cases} L_c = L - K - 2 \times T \tan \alpha \\ X_c = X + T \tan \alpha \end{cases}$	$\begin{cases} L_c = L - K - 2 \times T \tan \alpha \\ X_c = X + K + T \tan \alpha \end{cases}$

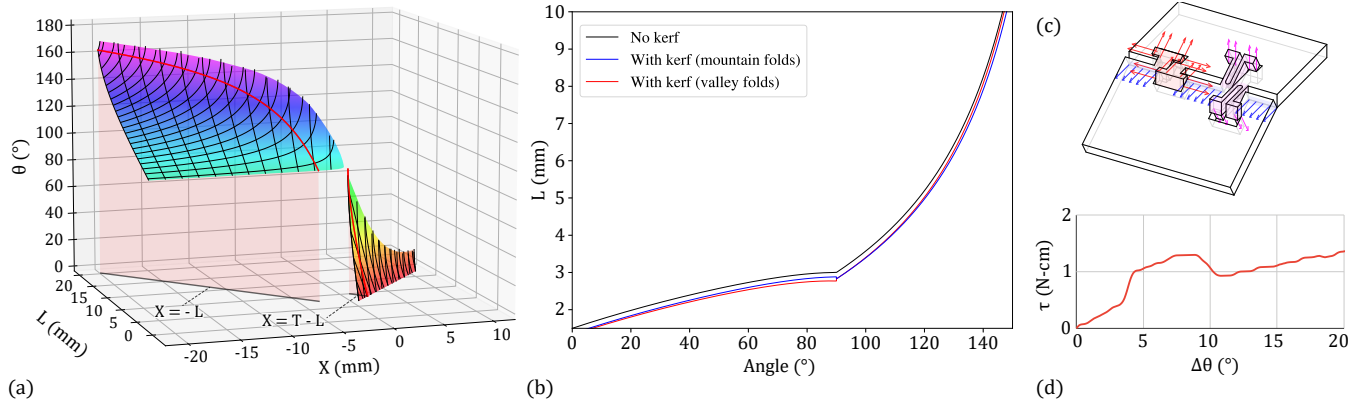


**Figure A.1:** (a) The solution space of  $<\theta$ -T-pattern from equation 3 with regard to  $\theta$ ,  $L$  and  $X$ . Multiple  $L$  and  $X$  pairs result in the same angle (the same color code). (b) With equation 3 and 4, the plot shows our achieved angle  $\theta$  relative to  $L$  for the  $<\theta$ -T-pattern. The plot also shows the parameters with and without correction for the kerf, where  $K = 0.12$  mm,  $\alpha = 2.1^\circ$  on a 3 mm-thick board). (c) The 2 types of T-patterns combined form an articulated joints. The arrows illustrates the force each component provides to achieve equilibrium. Force provided by  $<\theta$ -T-pattern is indicated by red arrows, force provided by  $>\theta$ -T-pattern is indicated by magenta arrows; and blue arrows indicate force along edge between the boards. (d) The torque-angle graph of the detent hinge, where  $\Delta\theta$  is the difference from the initial position.

## B FLATICULATION OBJECTS DETAILS

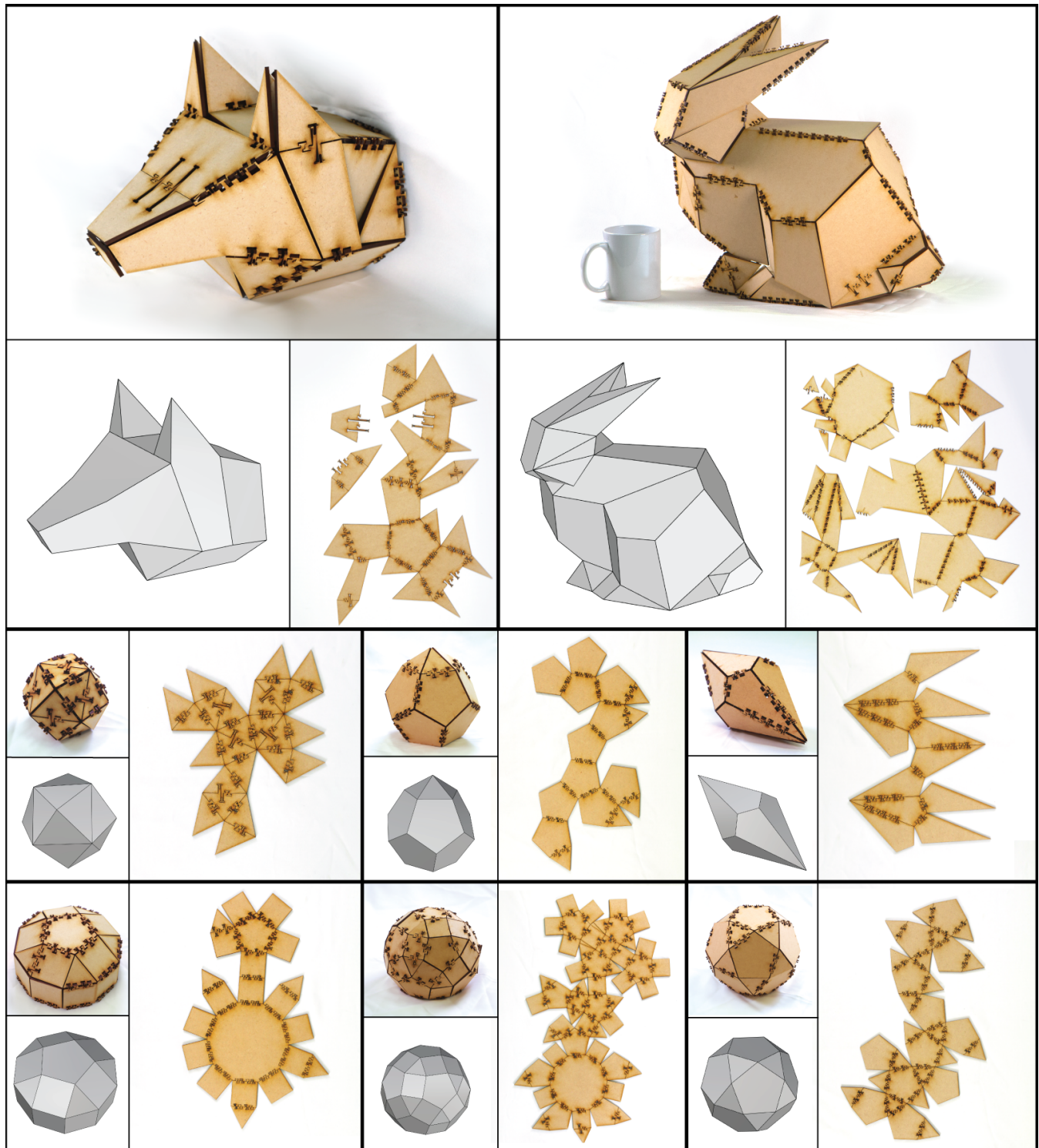


Figure B.1: Fabricated models of various 2-manifold models using Flaticulation along with the digital models and laser-cut pieces before assembly.

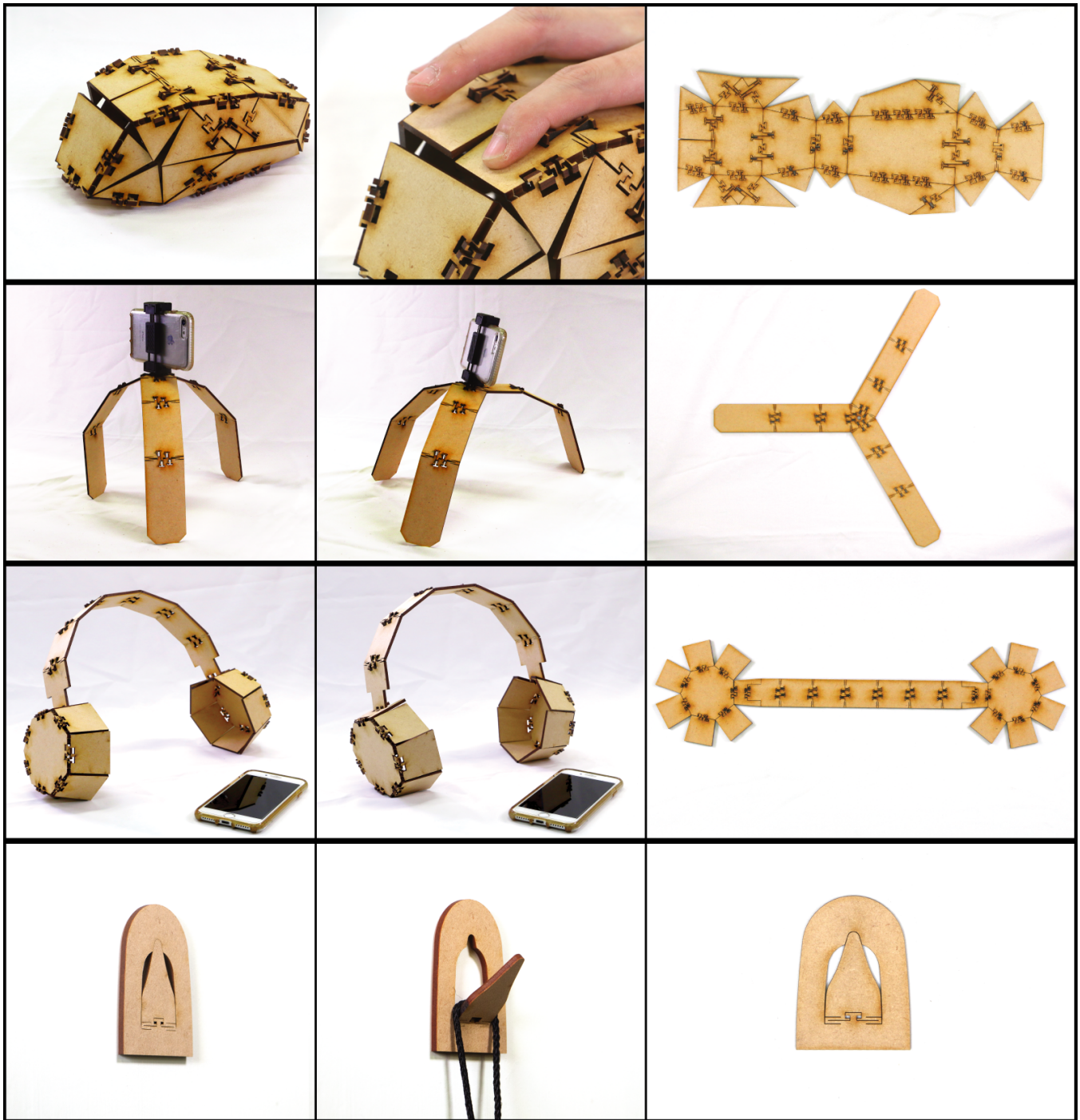


Figure B.2: Different configurations of the functional models with Flaticulation mechanisms and the laser-cut pieces before assembly.

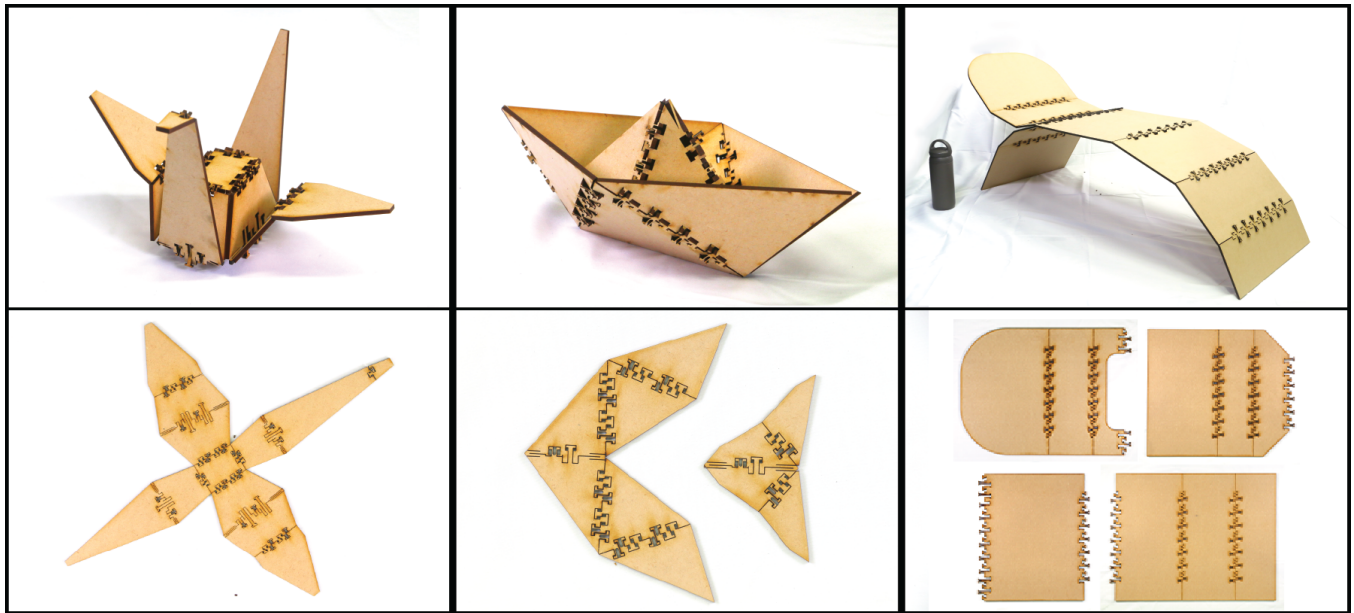


Figure B.3: Fabricated non-manifold models (origami-like models) using Flaticulation along with the digital models and laser-cut pieces before assembly.